LETTERS

Large-scale pattern growth of graphene films for stretchable transparent electrodes

Keun Soo Kim[1,3,4], Yue Zhao[7], Houk Jang[2], Sang Yoon Lee[5], Jong Min Kim[5], Kwang S. Kim[6], Jong-Hyun Ahn[2,3], Philip Kim[3,7], Jae-Young Choi[5] & Byung Hee Hong[1,3,4]

Problems associated with large-scale pattern growth of graphene constitute one of the main obstacles to using this material in device applications[1]. Recently, macroscopic-scale graphene films were prepared by two-dimensional assembly of graphene sheets chemically derived from graphite crystals and graphene oxides[2,3]. However, the sheet resistance of these films was found to be much larger than theoretically expected values. Here we report the direct synthesis of large-scale graphene films using chemical vapour deposition on thin nickel layers, and present two different methods of patterning the films and transferring them to arbitrary substrates. The transferred graphene films show very low sheet resistance of ~280 Ω per square, with ~80 per cent optical transparency. At low temperatures, the monolayers transferred to silicon dioxide substrates show electron mobility greater than 3,700 $cm^2 V^{-1} s^{-1}$ and exhibit the half-integer quantum Hall effect[4,5], implying that the quality of graphene grown by chemical vapour deposition is as high as mechanically cleaved graphene[6]. Employing the outstanding mechanical properties of graphene[7], we also demonstrate the macroscopic use of these highly conducting and transparent electrodes in flexible, stretchable, foldable electronics[8,9].

Graphene has been attracting much attention owing to its fascinating physical properties such as quantum electronic transport[4,5], a tunable band gap[10], extremely high mobility[11], high elasticity[7] and electromechanical modulation[12]. Since the discovery of the first isolated graphene prepared by mechanical exfoliation of graphite crystals[6], many chemical approaches to synthesize large-scale graphene have been developed, including epitaxial growth on silicon carbide (refs 13, 14) and ruthenium (ref. 15) as well as two-dimensional assembly of reduced graphene oxides[3,16–18] and exfoliated graphene sheets[2]. Epitaxial growth provides high-quality multilayer graphene samples interacting strongly with their substrates, but electrically isolated mono- or bilayer graphene for device applications has not been made. On the other hand, the self-assembly of soluble graphene sheets demonstrates the possibility of low-cost synthesis and the fabrication of large-scale transparent films. However, these assembled graphene films show relatively poor electrical conductivity owing to the poor interlayer junction contact resistance and the structural defects formed during the vigorous exfoliation and reduction processes. In this work, we develop a technique for growing few-layer graphene films using chemical vapour deposition (CVD) and successfully transferring the films to arbitrary substrates without intense mechanical and chemical treatments, to preserve the high crystalline quality of the graphene samples. Therefore, we expect to observe enhanced electrical and mechanical properties. The growth, etching and transferring processes of the CVD-grown large-scale graphene films are summarized in Fig. 1.

It has been known for over 40 years that CVD of hydrocarbons on reactive nickel or transition-metal-carbide surfaces can produce thin graphitic layers[19–21]. However, the large amount of carbon sources absorbed on nickel foils usually form thick graphite crystals rather than graphene films (Fig. 2a). To solve this problem, thin layers of nickel of thickness less than 300 nm were deposited on SiO_2/Si substrates using an electron-beam evaporator, and the samples were then heated to 1,000 °C inside a quartz tube under an argon atmosphere. After flowing reaction gas mixtures (CH_4:H_2:Ar = 50:65:200 standard cubic centimetres per minute), we rapidly cooled the samples to room temperature (~25 °C) at the rate of ~10 °C s^{-1} using flowing argon. We found that this fast cooling rate is critical in suppressing formation of multiple layers and for separating graphene layers efficiently from the substrate in the later process[20].

A scanning electron microscope (SEM; JSM6490, Jeol) image of graphene films on a thin nickel substrate shows clear contrast between areas with different numbers of graphene layers (Fig. 2a). Transmission electron microscope (TEM; JEM3010, Jeol) images (Fig. 2b) show that the film mostly consists of less than a few layers of graphene. After transfer of the film to a silicon substrate with a 300-nm-thick SiO_2 layer, optical and confocal scanning Raman microscope (CRM 200, Witech) images were made of the same area (Fig. 2c, d)[22]. The brightest area in Fig. 2d corresponds to monolayers, and the darkest area is composed of more than ten layers of graphene. Bilayer structures appear to predominate in both TEM and Raman images for this particular sample, which was prepared from 7 min of growth on a 300-nm-thick nickel layer. We found that the average number of graphene layers, the domain size and the substrate coverage can be controlled by changing the nickel thickness and growth time during the growth process (Supplementary Figs 1 and 2), thus providing a way of controlling the growth of graphene for different applications.

Atomic force microscope (AFM; Nanoscopes IIIa and E, Digital Instruments) images often show the ripple structures caused by the difference between the thermal expansion coefficients of nickel and graphene (Fig. 2c, inset; see also Supplementary Fig. 3)[19]. We believe that these ripples make the graphene films more stable against mechanical stretching[23], making the films more expandable, as we will discuss later. Multilayer graphene samples are preferable in terms of mechanical strength for supporting large-area film structures, whereas thinner graphene films have higher optical transparency. We find that a ~300-nm-thick nickel layer on a silicon wafer is the optimal substrate for the large-scale CVD growth that yields mechanically stable, transparent graphene films to be transferred and stretched after they are formed, and that thinner nickel layers with a shorter growth time yield predominantly mono- and bilayer graphene film for microelectronic device applications (Supplementary Fig. 1c).

[1]Department of Chemistry, [2]School of Advanced Materials Science and Engineering, [3]SKKU Advanced Institute of Nanotechnology, [4]Center for Nanotubes and Nanostructured Composites, Sungkyunkwan University, Suwon 440-746, Korea. [5]Samsung Advanced Institute of Technology, PO Box 111, Suwon 440-600, Korea. [6]Department of Chemistry, Pohang University of Science and Technology, Pohang 790-784, Korea. [7]Department of Physics, Columbia University, New York, New York 10027, USA.

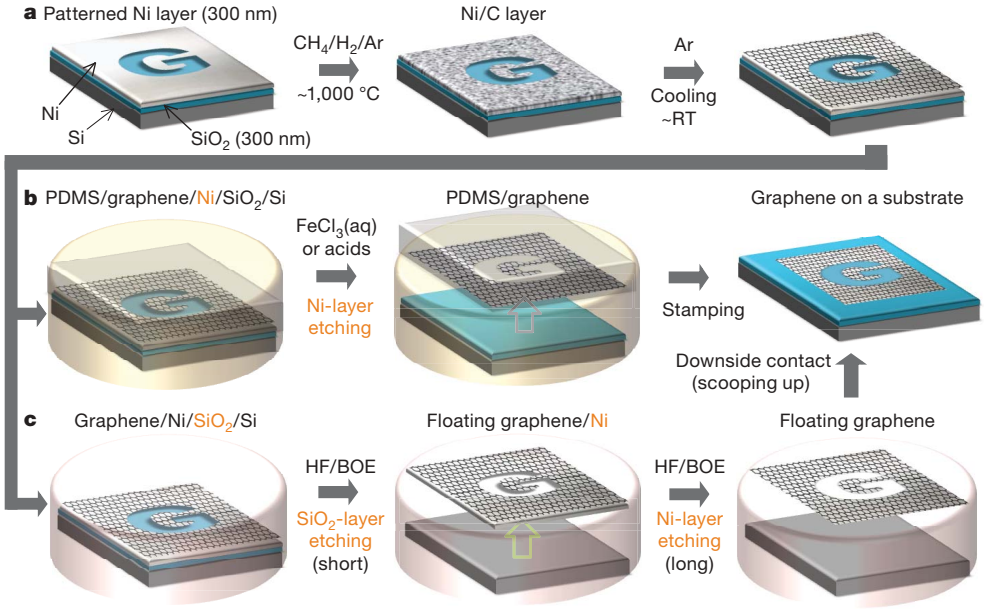

Figure 1 | Synthesis, etching and transfer processes for the large-scale and patterned graphene films. **a**, Synthesis of patterned graphene films on thin nickel layers. **b**, Etching using $FeCl_3$ (or acids) and transfer of graphene films using a PDMS stamp. **c**, Etching using BOE or hydrogen fluoride (HF) solution and transfer of graphene films. RT, room temperature (~25 °C).

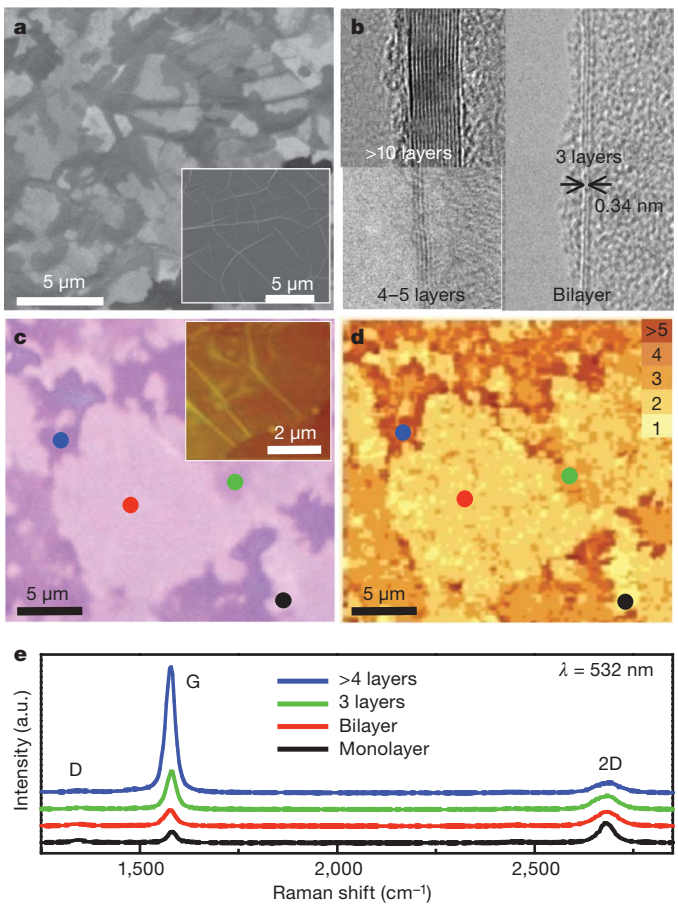

Figure 2 | Various spectroscopic analyses of the large-scale graphene films grown by CVD. **a**, SEM images of as-grown graphene films on thin (300-nm) nickel layers and thick (1-mm) Ni foils (inset). **b**, TEM images of graphene films of different thicknesses. **c**, An optical microscope image of the graphene film transferred to a 300-nm-thick silicon dioxide layer. The inset AFM image shows typical rippled structures. **d**, A confocal scanning Raman image corresponding to **c**. The number of layers is estimated from the intensities, shapes and positions of the G-band and 2D-band peaks. **e**, Raman spectra (532-nm laser wavelength) obtained from the corresponding coloured spots in **c** and **d**. a.u., arbitrary units.

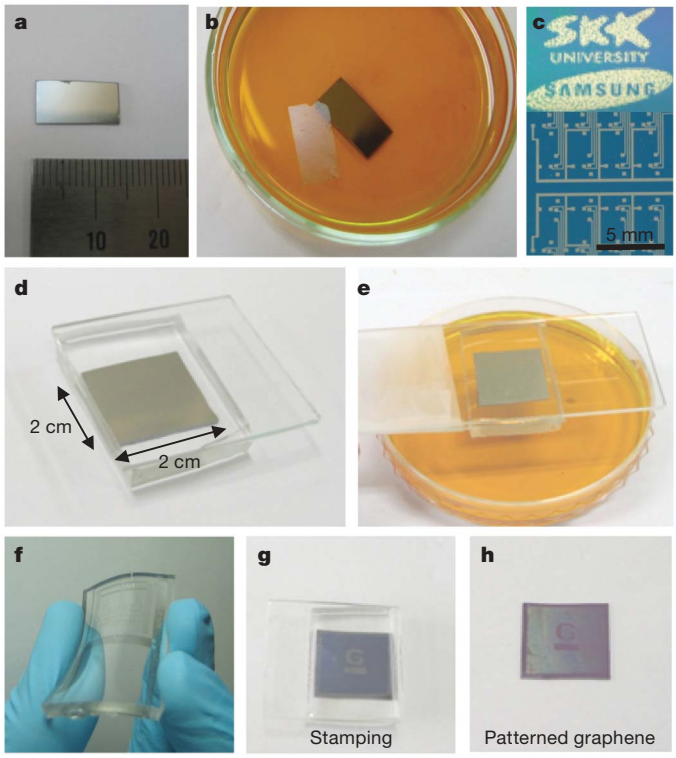

Figure 3 | Transfer processes for large-scale graphene films. **a**, A centimetre-scale graphene film grown on a Ni(300 nm)/SiO_2(300 nm)/Si substrate. **b**, A floating graphene film after etching the nickel layers in 1 M $FeCl_3$ aqueous solution. After the removal of the nickel layers, the floating graphene film can be transferred by direct contact with substrates. **c**, Various shapes of graphene films can be synthesized on top of patterned nickel layers. **d**, **e**, The dry-transfer method based on a PDMS stamp is useful in transferring the patterned graphene films. After attaching the PDMS substrate to the graphene (**d**), the underlying nickel layer is etched and removed using $FeCl_3$ solution (**e**). **f**, Graphene films on the PDMS substrates are transparent and flexible. **g**, **h**, The PDMS stamp makes conformal contact with a silicon dioxide substrate. Peeling back the stamp (**g**) leaves the film on a SiO_2 substrate (**h**).

Etching nickel substrate layers and transferring isolated graphene films to other substrates is important for device applications. Usually, nickel can be etched by strong acid such as HNO_3, which often produces hydrogen bubbles and damages the graphene. In our work, an aqueous iron (III) chloride ($FeCl_3$) solution (1 M) was used as an oxidizing etchant to remove the nickel layers. The net ionic equation of the etching reaction can be represented as follows:

$$2Fe^{3+}(aq) + Ni(s) \rightarrow 2Fe^{2+}(aq) + Ni^{2+}(aq)$$

This redox process slowly etches the nickel layers effectively within a mild pH range without forming gaseous products or precipitates. In a few minutes, the graphene film separated from the substrate floats on the surface of the solution (Fig. 3a, b), and the film is then ready to be transferred to any kind of substrate. Use of buffered oxide etchant (BOE) or hydrogen fluoride solution removes silicon dioxide layers, so the patterned graphene and the nickel layer float together on the solution surface. After transfer to a substrate, further reaction with BOE or hydrogen fluoride solution completely removes the remaining nickel layers (Supplementary Fig. 5).

We also develop a dry-transfer process for the graphene film using a soft substrate such as polydimethylsiloxane (PDMS) stamp[24]. Here we first attach the PDMS stamp to the CVD-grown graphene film on the nickel substrate (Fig. 3d). The nickel substrate can be etched away using $FeCl_3$ as described above, leaving the adhered graphene film on the PDMS substrate (Fig. 3e). By using the pre-patterned nickel substrate (Fig. 3c), we can transfer various sizes and shapes of graphene film to an arbitrary substrate. This dry-transfer process turns out to be very useful in making large-scale graphene electrodes and devices without additional lithography processes (Fig. 3f–h). Microscopically, these few-layer transferred graphene films often show linear crack patterns with an angle of 60° or 120°, indicating a particular crystallographic edge with large crystalline domains (Supplementary Fig. 1b)[25]. In addition, the Raman spectra measured for graphene films on nickel substrates show a strongly suppressed defect-related D-band peak (Supplementary Fig. 3). This D peak grows only slightly after the transfer process (Fig. 2e), indicating overall good quality of the resulting graphene film. Further optimization of the transfer process with substrate control makes possible transfer yields approaching 99% (Supplementary Table 1).

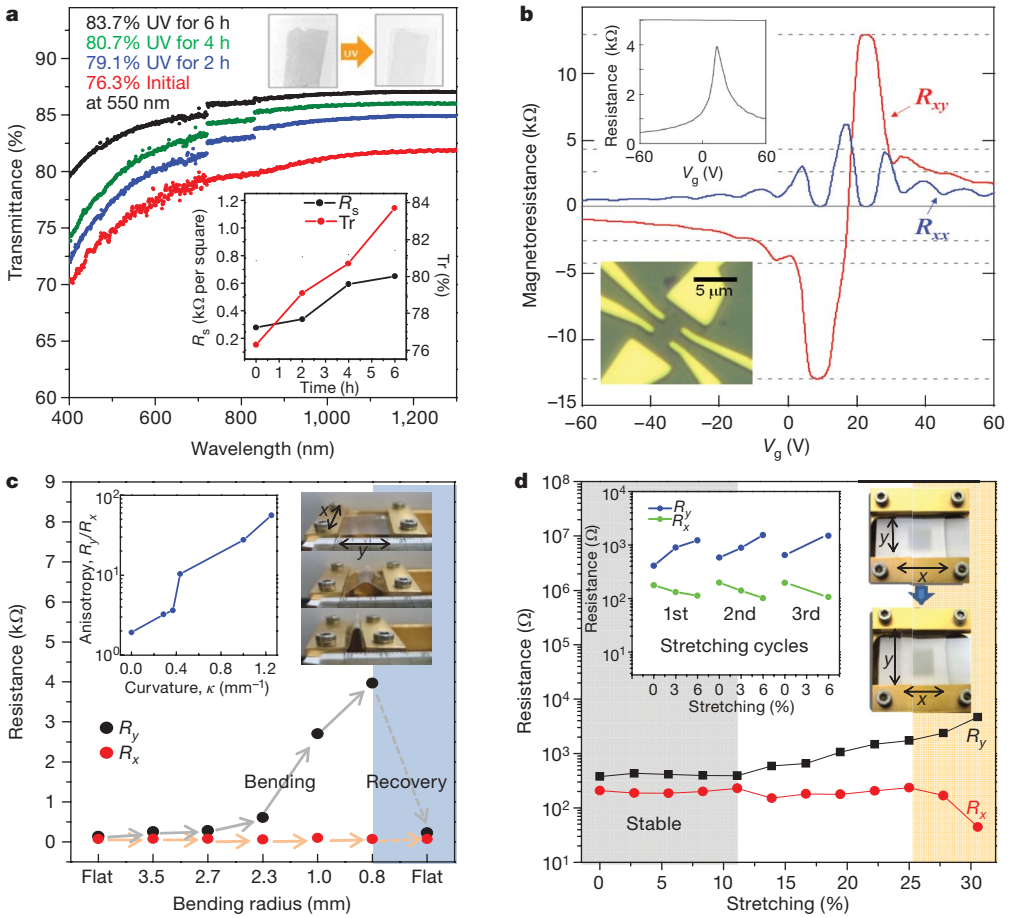

Figure 4 | Optical and electrical properties of the graphene films. **a**, Transmittance of the graphene films on a quartz plate. The discontinuities in the absorption curves arise from the different sensitivities of the switching detectors. The upper inset shows the ultraviolet (UV)-induced thinning and the consequent enhancement of transparency. The lower inset shows the changes in transmittance, Tr, and sheet resistance, R_s, as functions of ultraviolet illumination time. **b**, Electrical properties of monolayer graphene devices showing the half-integer quantum Hall effect and high electron mobility. The upper inset shows a four-probe electrical resistance measurement on a monolayer graphene Hall bar device (lower inset) at 1.6 K. We apply a gate voltage, V_g, to the silicon substrate to control the charge density in the graphene sample. The main panel shows longitudinal (R_{xx}) and transverse (R_{xy}) magnetoresistances measured in this device for a magnetic field $B = 8.8$ T. The monolayer graphene quantum Hall effect is clearly observed, showing the plateaux with filling factor $\nu = 2$ at $R_{xy} = (2e^2/h)^{-1}$ and zeros in R_{xx}. (Here e is the elementary charge and h is Planck's constant.) Quantum Hall plateaux (horizontal dashed lines) are developing for higher filling factors. **c**, Variation in resistance of a graphene film transferred to a ~0.3-mm-thick PDMS/PET substrate for different distances between holding stages (that is, for different bending radii). The left inset shows the anisotropy in four-probe resistance, measured as the ratio, R_y/R_x, of the resistances parallel and perpendicular to the bending direction, y. The right inset shows the bending process. **d**, Resistance of a graphene film transferred to a PDMS substrate isotropically stretched by ~12%. The left inset shows the case in which the graphene film is transferred to an unstretched PDMS substrate. The right inset shows the movement of holding stages and the consequent change in shape of the graphene film.

For the macroscopic transport electrode application, the optical and electrical properties of $1 \times 1\ cm^2$ graphene films were respectively measured by ultraviolet–visible spectrometer and four-probe Van der Pauw methods (Fig. 4a, b). We measured the transmittance using an ultraviolet–visible spectrometer (UV-3600, Shimazdu) after transferring the floating graphene film to a quartz plate (Fig. 4a). In the visible range, the transmittance of the film grown on a 300-nm-thick nickel layer for 7 min is ~80%, a value similar to those found for previously studied assembled films[2,3]. Because the transmittance of an individual graphene layer is ~2.3% (ref. 26), this transmittance value indicates that the average number of graphene layers is six to ten. The transmittance can be increased to ~93% by further reducing the growth time and nickel thickness, resulting in a thinner graphene film (Supplementary Fig. 1). Ultraviolet/ozone etching (ultraviolet/ozone cleaner, 60 W, BioForce) is also useful in controlling the transmittance in an ambient condition (Fig. 4a, upper inset). Indium electrodes were deposited on each corner of the square (Fig. 4a, lower inset) to minimize contact resistance. The minimum sheet resistance is ~280 Ω per square, which is ~30 times smaller than the lowest sheet resistance measured on assembled films[2,3]. The values of sheet resistance increase with the ultraviolet/ozone treatment time, in accordance with the decreasing number of graphene layers (Fig. 4a).

For microelectronic application, the mobility of the graphene film is critical. To measure the intrinsic mobility of a single-domain graphene sample, we transferred the graphene samples from a PDMS stamp to a degenerate doped silicon wafer with a 300-nm-deep thermally grown oxide layer. Monolayer graphene samples were readily located on the substrate from the optical contrast[26] and their identification was subsequently confirmed by Raman spectroscopy[22]. Electron-beam lithography was used to make multi-terminal devices (Fig. 4b, lower inset). Notably, the multi-terminal electrical measurements showed that the electron mobility is ~3,750 $cm^2\,V^{-1}\,s^{-1}$ at a carrier density of ~$5 \times 10^{12}\ cm^{-2}$ (Fig. 4b). For a high magnetic field of 8.8 T, we observe the half-integer quantum Hall effect (Fig. 4b) corresponding to monolayer graphene[4,5], indicating that the quality of CVD-grown graphene is comparable to that of mechanically cleaved graphene (Supplementary Fig. 6)[6].

In addition to the good optical and electrical properties, the graphene film has excellent mechanical properties when used to make flexible and stretchable electrodes (Fig. 4c, d)[7]. We evaluated the foldability of the graphene films transferred to a polyethylene terephthalate (PET) substrate (thickness, ~100 μm) coated with a thin PDMS layer (thickness, ~200 μm; Fig. 4c) by measuring resistances with respect to bending radii. The resistances show little variation up to the bending radius of 2.3 mm (approximate tensile strain of 6.5%) and are perfectly recovered after unbending. Notably, the original resistance can be restored even for the bending radius of 0.8 mm (approximate tensile strain of 18.7%), exhibiting extreme mechanical stability in comparison with conventional materials used in flexible electronics[27].

The resistances of graphene films transferred to pre-strained and unstrained PDMS substrates were measured with respect to uniaxial tensile strain ranging from 0 to 30% (Fig. 4d). Similar to the results in the folding experiment, the transferred film on an unstrained substrate recovers its original resistance after stretching by ~6% (Fig. 4d, left inset). However, further stretching often results in mechanical failure. Thus, we tried to transfer the film to pre-strained substrates[28] to enhance the electromechanical stabilities by creating ripples similar to those observed in the growth process (Fig. 2c, inset; Supplementary Fig. 4). The graphene transferred to a longitudinally strained PDMS substrate does not show much enhancement, owing to the transverse strain induced by Poisson's effect[29]. To prevent this problem, the PDMS substrate was isotropically stretched by ~12% before transferring the film to it (Fig. 4d). Surprisingly, both longitudinal and transverse resistances (R_y and R_x) appear stable up to ~11% stretching and show only one order of magnitude change at ~25% stretching. We suppose that further uniaxial stretching can change the electronic band structures of graphene, leading to the modulation of the sheet resistance. These electromechanical properties thus show our graphene films to be not only the strongest[7] but also the most flexible and stretchable conducting transparent materials so far measured[26].

In conclusion, we have developed a simple method to grow and transfer high-quality stretchable graphene films on a large scale using CVD on nickel layers. The patterned films can easily be transferred to stretchable substrates by simple contact methods, and the number of graphene layers can be controlled by varying the thickness of the catalytic metals, the growth time and/or the ultraviolet treatment time. Because the dimensions of the graphene films are limited simply by the size of the CVD growth chamber, scaling up can be readily achieved, and the outstanding optical, electrical and mechanical properties of the graphene films enable numerous applications including use in large-scale flexible, stretchable, foldable transparent electronics[8,9,30].

Received 5 October; accepted 8 December 2008.
Published online 14 January 2009.

1. Geim, A. K. & Novoselov, K. S. The rise of graphene. *Nature Mater.* **6,** 183–191 (2007).
2. Li, X. *et al.* Highly conducting graphene sheets and Langmuir–Blodgett films. *Nature Nanotechnol.* **3,** 538–542 (2008).
3. Eda, G., Fanchini, G. & Chhowalla, M. Large-area ultrathin films of reduced graphene oxide as a transparent and flexible electronic material. *Nature Nanotechnol.* **3,** 270–274 (2008).
4. Novoselov, K. S. *et al.* Two-dimensional gas of massless Dirac fermions in graphene. *Nature* **438,** 197–200 (2005).
5. Zhang, Y., Tan, J. W., Stormer, H. L. & Kim, P. Experimental observation of the quantum Hall effect and Berry's phase in graphene. *Nature* **438,** 201–204 (2005).
6. Novoselov, K. S. *et al.* Electric field effect in atomically thin carbon films. *Science* **306,** 666–669 (2004).
7. Lee, C., Wei, X., Kysar, J. W. & Hone, J. Measurement of the elastic properties and intrinsic strength of monolayer graphene. *Science* **321,** 385–388 (2008).
8. Kim, D.-H. *et al.* Stretchable and foldable silicon integrated circuits. *Science* **320,** 507–511 (2008).
9. Sekitani, T. *et al.* A rubberlike stretchable active matrix using elastic conductors. *Science* **321,** 1468–1472 (2008).
10. Han, M. Y., Oezyilmaz, B., Zhang, Y. & Kim, P. Energy band gap engineering of graphene nanoribbons. *Phys. Rev. Lett.* **98,** 206805 (2007).
11. Bolotin, K. I. *et al.* Ultrahigh electron mobility in suspended graphene. *Solid State Commun.* **146,** 351–355 (2008).
12. Bunch, J. S. *et al.* Electromechanical resonators from graphene sheets. *Science* **315,** 490–493 (2008).
13. Ohta, T., Bostwick, A., Seyller, T., Horn, K. & Rotenberg, E. Controlling the electronic structure of bilayer graphene. *Science* **313,** 951–954 (2006).
14. Berger, C. *et al.* Electronic confinement and coherence in patterned epitaxial graphene. *Science* **312,** 1191–1196 (2006).
15. Sutter, P. W., Flege, J.-I. & Sutter, E. A. Epitaxial graphene on ruthenium. *Nature Mater.* **7,** 406–411 (2008).
16. Dikin, D. A. *et al.* Preparation and characterization of graphene oxide paper. *Nature* **448,** 457–460 (2007).
17. Stankovich, S, *et al.* Graphene-based composite materials. *Nature* **442,** 282–286 (2006).
18. Li, D., Muller, M. B., Gilje, S., Kaner, R. B. & Wallace, G. G. Processable aqueous dispersions of graphene nanosheets. *Nature Nanotechnol.* **3,** 101–105 (2008).
19. Obraztsov, A. N., Obraztsova, E. A., Tyurnina, A. V. & Zolotukhin, A. A. Chemical vapor deposition of thin graphite films of nanometer thickness. *Carbon* **45,** 2017–2021 (2007).
20. Yu, Q, *et al.* Graphene segregated on Ni surfaces and transferred to insulators. *Appl. Phys. Lett.* **93,** 113103 (2008).
21. Reina, A. *et al.* Large area, few-layer graphene films on arbitrary substrates by chemical vapor deposition. *Nano Lett.* article ASAP at ⟨http://pubs.acs.org/doi/abs/10.1021/nl801827v⟩ (2008).
22. Ferrari, A. C. *et al.* Raman spectrum of graphene and graphene layers. *Phys. Rev. Lett.* **97,** 187401 (2006).
23. Khang, D.-Y. *et al.* Individual aligned single-wall carbon nanotubes on elastomeric substrates. *Nano Lett.* **8,** 124–130 (2008).
24. Yang, P. *et al.* Mirrorless lasing from mesostructured waveguides patterned by soft lithography. *Science* **287,** 465–467 (2000).
25. Li, X., Wang, X., Zhang, L., Lee, S. & Dai, H. Chemically derived, ultrasmooth graphene nanoribbon semiconductors. *Science* **319,** 1229–1232 (2008).
26. Nair, R. R. *et al.* Fine structure constant defines visual transparency of graphene. *Science* **320,** 1308 (2008).
27. Lewis, J. Material challenge for flexible organic devices. *Mater. Today* **9,** 38–45 (2006).
28. Sun, Y., Choi, W. M., Jiang, H., Huang, Y. Y. & Rogers, J. A. Controlled buckling of semiconductor nanoribbons for stretchable electronics. *Nature Nanotechnol.* **1,** 201–207 (2006).

29. Khang, D.-Y., Jiang, H., Huang, Y. & Rogers, J. A. A stretchable form of single-crystal silicon for high-performance electronics on rubber substrates. *Science* **311,** 208–212 (2006).
30. Ko, H. C. *et al.* A hemispherical electronic eye camera based on compressible silicon optoelectronics. *Nature* **454,** 748–753 (2008).

Supplementary Information is linked to the online version of the paper at www.nature.com/nature.

Acknowledgements We thank J. H. Han, J. H. Kim, H. Lim, S. K. Bae and H.-J. Shin for assisting in graphene synthesis and analysis. This work was supported by the Korea Science and Engineering Foundation grant funded by the Korea Ministry for Education, Science and Technology (Center for Nanotubes and Nanostructured Composites R11-2001-091-00000-0), the Global Research Lab programme (Korea Foundation for International Cooperation of Science and Technology), the Brain Korea 21 project (Korea Research Foundation) and the information technology research and development programme of the Korea Ministry of Knowledge Economy (2008-F024-01).

Author Contributions B.H.H. planned and supervised the project; J.-Y.C. supported and assisted in supervision on the project; S.Y.L, J.M.K. and K.S.K. advised on the project; K.S.K. and B.H.H. designed and performed the experiments; B.H.H., P.K., J.-H.A and K.S.K. analysed data and wrote the manuscript; Y.Z. and P.K. made the quantum Hall devices and the measurements; and H.J. and J.-H.A. helped with the transfer process and the electromechanical analyses.

Author Information Reprints and permissions information is available at www.nature.com/reprints. Correspondence and requests for materials should be addressed to B.H.H. (byunghee@skku.edu) or J.-Y.C. (jaeyoung88.choi@samsung.com).